A textural examination of the Yamato 980459 and Los Angeles shergottites using crystal size distribution analysis

Rachel C. F. Lentz* and Harry Y. McSween, Jr.

Department of Earth & Planetary Sciences, University of Tennessee, Knoxville, TN 37996-1410, U.S.A.
Corresponding author. E-mail: rcflentz@higp.hawaii.edu

Abstract: The basaltic shergottite group is the most plentiful of the Martian meteorite types. Within that compositional category are three distinct textural groups, each suggesting distinct crystallization histories. We present results of a textural study, using crystal size distribution (CSD) analysis, of Yamato (Y) 980459 and Los Angeles, the most primitive and evolved shergottites respectively, and we compare these results to previous CSD work on basaltic shergottites.

Y980459 resembles picritic shergottites (*e.g.* DaG 476), with large zoned olivine set in a groundmass dominated by orthopyroxene. It is unique in having a glassy mesostasis with dendritic olivine and pyroxene, rather than maskelynite. Los Angeles resembles other co-saturated shergottites (*e.g.* QUE 94201) with a subophitic intergrowth of zoned clinopyroxene and maskelynite.

CSD results show Y980459 pyroxenes grew in one stage of steady-state nucleation and growth, cooling at 3–7℃/hr. A CSD of the olivine population suggests slower cooling rates during megacryst formation with an increase during groundmass olivine growth, probably reflecting magma ascent. A CSD plot of Los Angeles pyroxenes shows a smooth downward curvature, also noted in previous analyses of QUE 94201 and EETA79001B. The plot reflects co-crystallization of plagioclase and pyroxene, and supports a single continuous interval of growth.

key words: basaltic shergottites, crystal size distribution, Yamato 980459, Los Angeles

1. Introduction

Of all the Martian meteorite lithologies, the basaltic shergottite group has grown the most, with new samples found every year. Previously, we examined the mineral textures of several of the basaltic shergottites (Lentz and McSween, 2000) in an attempt to reveal details of their crystallization histories. Two more recent finds, Yamato 980459 (Misawa, 2003; Mikouchi *et al*., 2003) and Los Angeles (Stones 1 and 2) (Rubin *et al*., 2000) have unusual compositional aspects compared with the traditional basaltic shergottites, prompting the question of whether, and how, their crystallization histories might differ from the rest of the group. We here present our results of an examination of the Los Angeles and Y980459 textures, applying the same quantitative approach we used on other shergottites (crystal size distribution analysis) and comparing the results

to our previous assessments of shergottite crystallization histories.

2. Petrographic background

All the basaltic shergottites are dominated by two clinopyroxenes (pigeonite and augite), usually zoned (*e.g.*, McCoy *et al*., 1992; McSween *et al*., 1996), with variable amounts of plagioclase, which has been shock converted to maskelynite. With the larger number of samples, there now appear to be three well-defined textural subgroups, which also generally reflect their bulk chemical composition.

The first group is represented by Shergotty, Zagami, and now NWA 480 and 856 (Stolper and McSween, 1979; Grossman and Zipfel, 2001; Jambon *et al*., 2002).   These meteorites all exhibit fine- to medium-grained, partially cumulus textures (Fig. 1a) interpreted as resulting from the crystallization of two pyroxenes for a long temperature interval before plagioclase joined the liquidus and grew interstitially (*e.g.* Stolper and McSween, 1979; McCoy *et al*., 1992; Hale *et al*., 1999).   In contrast, the second group exhibits medium-grained subophitic textures (Fig. 1b) representing the co-crystallization of pyroxene and plagioclase (now maskelynite) over most of the crystallization interval.   Mineral modes and bulk compositions reflect this greater abundance of original plagioclase than in the first group (Meyer, 2003).   The meteorites that fit in this category are EETA79001 lithology B, QUE 94201, Dhofar 378, and NWA 1669 (Steele and Smith, 1982; McSween *et al*., 1996; Ikeda *et al*., 2002; Jambon *et al*., 2003).

The third textural group, called the olivine-phyric (Goodrich, 2002) or picritic (Barrat *et al*., 2002) shergottites, has greatly expanded, particularly from the hot desert finds.   For many years only EETA79001 lithology A exhibited this lithology, but now it is joined by DaG 476, SaU 005, Dhofar 019, NWA 1068, and NWA 1195 and their respective paired meteorites (Steele and Smith, 1982; Zipfel, 2000; Zipfel *et al*., 2000; Taylor *et al*., 2000; Barrat *et al*., 2002; Irving *et al*., 2002).   These meteorites all have fine-grained groundmasses composed of zoned pyroxene laths (pigeonite and augite) and interstitial maskelynite, with megacrysts of Mg-rich olivine ($\pm$chromite$\pm$ orthopyroxene; Fig. 1c).   In some cases, there is an additional population of finer-grained olivine of more Fe-rich composition (*e.g.* Dhofar 019; Taylor *et al*., 2002).

Most basaltic shergottites have been interpreted as representing surface flows or shallow intrusions, although there are indications that some experienced crystallization of pyroxene or olivine cores at depth before the magma rose to the surface and crystallized further (McCoy *et al*., 1992; Wadhwa *et al*., 1994; Lentz and McSween, 2000).

2.1. *Yamato 980459*

Yamato 980459 falls into the picritic shergottite category, with a fine-grained pyroxene dominated groundmass and Mg-rich megacrysts of olivine (Fig. 2a), although it also displays a host of smaller olivine grains comparable in size to the pyroxene of the groundmass (Greshake *et al*., 2004).   In contrast to the other picritic shergottites, these groundmass pyroxenes are dominated by orthopyroxene cores, with only thin rims of pigeonite and augite.   Typically, pigeonite and augite dominate the groundmass pyroxenes in the picritic shergottites, and orthopyroxene is only present in the megacryst
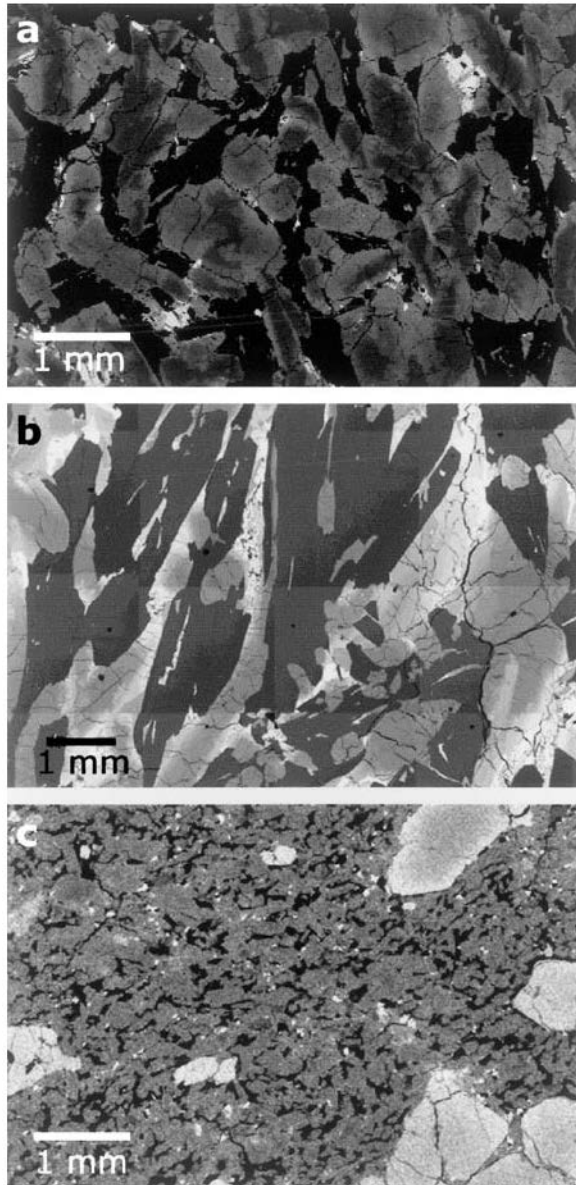
Fig. 1. Three textural groups of basaltic shergottites in BSEs. a) Texture of Shergotty with medium-grained, zoned pyroxene (dark to light gray) and later-stage interstitial maskelynite (black). b) Subophitic texture of QUE 94201 from co-crystallization of zoned pyroxene (gray) and plagioclase (now maskelynite, dark gray). c) Porphyritic texture of picritic shergottite DaG 476 with megacrysts of olivine (light gray) and a finer groundmass of pyroxene (medium gray) and interstitial maskelynite (black).
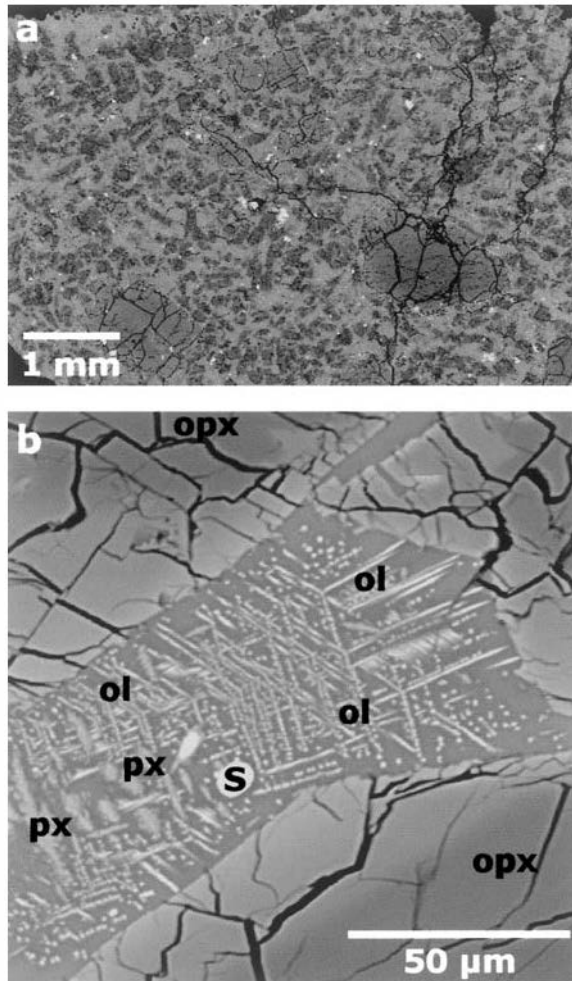
Fig. 2. Yamato 980459 textures. a) General picritic texture with olivine megacrysts and a ground-mass of zoned orthopyroxene and smaller olivine. b) Close-up image of glassy mesostasis interstitial to orthopyroxene (opx), with dendritic olivine (ol), clinopyroxene (px), and sulfide droplets (s).

populations (*e.g.* EETA79001A, DaG 476). Y980459 also differs in that the melt interstitial to the groundmass pyroxene and finer olivine never crystallized into plagio-clase or other late-stage phases (*e.g.* phosphates, Ti-rich oxides).   Instead, the melt was quenched and contains only dendritic olivine, chain-like augite, and sulfide droplets embedded in the glassy matrix (Fig. 2b; McKay *et al*., 2004; Greshake *et al*., 2004), although compositionally the melt is high in alkalis and silica and primed to crystallize plagioclase.

Unlike the olivine in some of the picritic shergottites (*e.g.* EETA79001A), the megacrysts of Y980459 closely match the core compositions expected to crystallize from
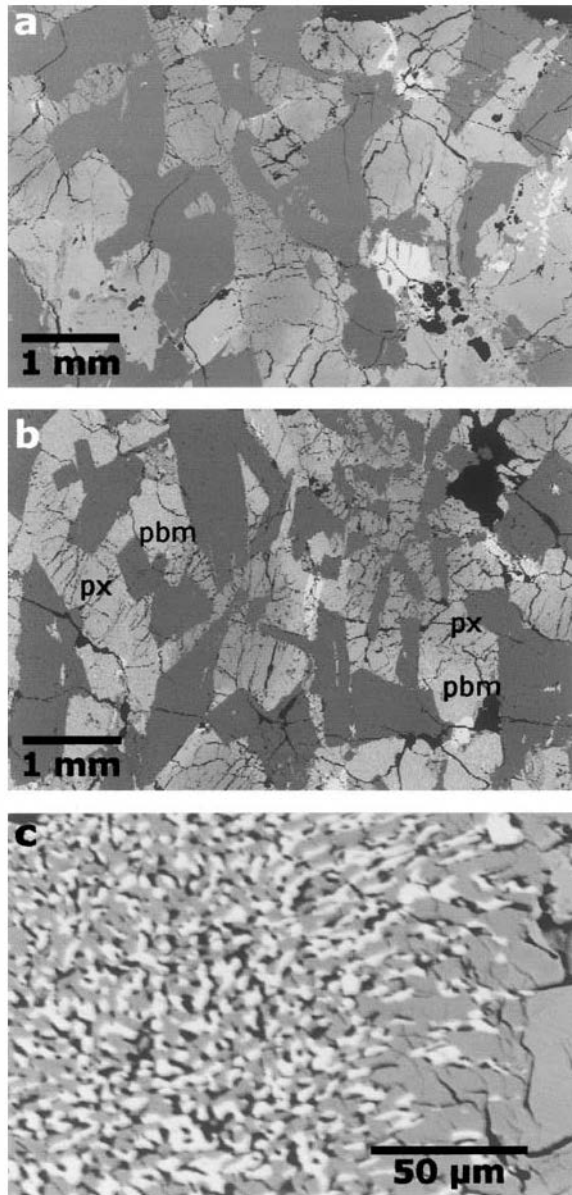
Fig. 3.   *General textures of Los Angeles.   a) Stone 1.   b) Stone 2.   Note that visually, Stone 2 appears slightly finer grained (images to same scale: 6 mm FOV).   Example pyroxene (px) and pyroxferroite breakdown material (PBM) have been labelled to illustrate contrast.   c) Close-up image of PBM showing intergrowth of silica (black), fayalite (white), and Fe-rich augite (gray).   Note the gradual shift to pyroxene towards the right of the image.*

the bulk rock composition, suggesting they are phenocrysts rather than xenocrysts (Koizumi *et al*., 2004; Greshake *et al*., 2004) and that Y980459 is the most primitive of all the known basaltic shergottites. The smaller olivine population is in equilibrium with the groundmass pyroxene, suggesting the two phases grew in place and concurrently. These compositional factors as well as other textural observations led Greshake *et al*. (2004) to propose a simple two-stage crystallization history for Y980459, with megacryst and orthopyroxene cores grown at depth, followed by rapid ascent and eruption onto the surface, where rims grew and interstitial melt quenched.

2.2. *Los Angeles*

Los Angeles is a multiply saturated basaltic shergottite, similar to QUE 94201 and EETA79001B, with a subophitic texture of intergrown zoned pyroxene and plagioclase (now maskelynite). Los Angeles is represented by two stones (Fig. 3a, b), found together, with similar enough textures and compositions that they were paired, but with subtle differences which imply they probably experienced slightly different crystallization conditions within the same parental magmatic body (Warren *et al*., 2004). Together, the stones represent the most evolved geochemistry of all the Martian meteorites (Rubin *et al*., 2000), which is most obviously exhibited mineralogically by the abundant patches of pyroxferroite breakdown material (PBM; Fig. 3c), a late, Fe-enriched intergrowth of ferroan augite, fayalite, and silica (Rubin *et al*., 2000). The primary differences between the two stones is that Stone 2 is slightly finer grained and more evolved compositionally: it displays a greater modal abundance of PBM, a more Fe-enriched bulk composition, and higher concentrations of light REE and several incompatible elements (*e.g.* K, Ti, P; Warren *et al*., 2004). Warren *et al*. (2004) speculate that these differences are attributable to a mild degree of compaction of the crystal mush once the flow was emplaced, adding 20% more mafic crystals to the area of Stone 1 or pressing 20 wt% late-stage melt into the area of Stone 2. Such a minor degree of late-stage melt migration is not uncommon in basaltic flows (*e.g.* Helz *et al*., 1989; Philpotts *et al*., 1996).

3. Method: Crystal size distribution (CSD) analysis

3.1. *CSD theory*

Crystal size distribution (CSD) analysis has been used to determine crystallization conditions and processes in a variety of terrestrial studies (*e.g*., Cashman and Marsh, 1988; Mangan *et al*., 1993), and based on the success of applying it to the nakhlites (Friedman-Lentz *et al*., 1999), we used it to analyze several of the basaltic shergottites (Lentz and McSween, 2000). The method applied here has been described in detail by Marsh (1988, 1998), Cashman and Marsh (1988), and in our previous paper (Lentz and McSween, 2000).

The theory is based on the idea of a crystallizing system achieving steady-state conditions, where continuous nucleation and growth produce a stable, skewed Gaussian distribution of grain sizes. The sizes of the grains in a population are all measured, generating a cumulative histogram. This then yields the number density (n) for each bin from $n = dN/dL$, or the change in slope of the cumulative curve grain number
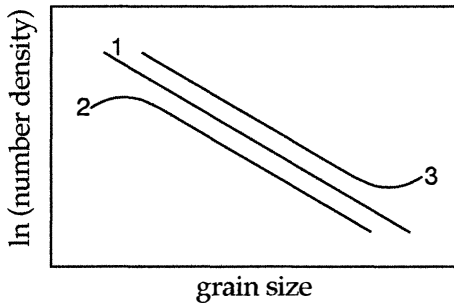
Fig. 4.   Example curve shapes for CSD plots.   Line 1 illustrates steady-state conditions of nucleation and growth.   Line 2 shows a depletion of small grains due to Ostwald ripening or population growth with no new nucleation.   Line 3 displays an overabundance of large grains, perhaps due to phenocryst accumulations.

(Cashman and Marsh, 1988).   The bin size is chosen so as to have a reasonable number of grains in each of the bins (although this will inevitably fall off at the higher grain sizes).   When grain size is plotted *versus* the natural log of this number density, the shape of the resulting CSD plot indicates the processes associated with formation of that grain population (Fig. 4).   If steady-state conditions were achieved, with continuous nucleation and growth, the plot should show an inverse log-linear relationship (a straight line of negative slope; Fig. 4, line 1).   Any deviations from linearity suggest the involvement of other geologic processes.

For example, a turnover at the smallest grain sizes (Fig. 4, line 2) may represent a complete cessation of nucleation with continued population growth.   In such a case, the smallest grains will grow into the next largest bin sizes, but with no replacements produced by nucleation, thereby depleting the smallest bins and producing the turnover. In contrast, a turn-up at the largest grain sizes (Fig. 4, line 3) implies an excess of large grains, perhaps due to an accumulation of large phenocrysts.   Conversely, a drop-off at the largest sizes may result from the loss of large grains by crystal settling (Marsh, 1988), or inhibition of further crystal growth due to lack of space or appropriate materials.

3.2. Analysis technique

Most basaltic shergottites are dominated by pyroxene as the sole liquidus phase for a long temperature interval, so pyroxene grains reveal the most about the crystallization conditions.   We therefore focused on measuring pyroxene grains in these meteorites, although the concurrent growth of small olivine grains in Y980459 prompted us to include that phase as well.   In order to minimize the geometric bias in measuring the elongate grains in a 2-dimensional thin section, we chose to define grain size by width (Friedman, 1998).

Practically, making measurements of shergottite pyroxene grains can be non-trivial: shock effects, from blurred grain boundaries to disrupted grains, required subjective width delineations in some cases, particularly in Los Angeles.   For Los Angeles, measurements were made on Fe-distribution maps or BSE images, but grain boundaries were verified using transmitted light microscopy.   In the case of Los Angeles Stone 1, three non-sequential thin sections (LA8hL, ME3277,1 and ME3277,2) were measured to ensure a sufficient number of grains (313) for statistically significant results.   For Los Angeles Stone 2, only one thin section was available (LA–745), but an imaged

subsection of it yielded 169 pyroxene grains. Since Stone 2 has a much greater abundance of PBM, and only true pyroxene grains were being analyzed, measurements were made on a Si-distribution map with reference to transmitted light images and a combined Fe-Ca-Si distribution map to verify grain boundaries and avoid PBM patches.

For Y980459, the pyroxene groundmass was much finer grained so posed no problem, statistically, with 1657 grains measured from only half the available thin section (Y980459,51-2). Measurements were made on a transmitted light mosaic but with reference to a combined image of back-scattered electrons and Ca and Si elemental distribution maps to differentiate small olivine grains from orthopyroxene grains. Full grain widths were measured since clinopyroxene rims are quite thin, and the minor number of free-standing clinopyroxene grains were also included in the overall measurements. Olivine grains were measured separately, and totalled 171 over the entire thin section, including four large megacrysts, which are substantially bigger than the smaller, groundmass olivine.

4. Results

Numerical results from CSD measurements are presented in Table 1, with previously acquired data (Lentz and McSween, 2000; Lentz *et al.*, 2001) for other shergottites included for comparison. All line fits were generated using a weighted least squares algorithm. Weighting is based on the error associated with the number of grains represented by each data point (*i.e.* more grains means lower error). In general, the shapes of CSD plots of Y980459 and the two Los Angeles stones fit well with those of other shergottites of similar textures.

Table 1. *Crystal Size Distribution data for basaltic shergottites.*

Meteorite	Avg width (mm)	St. dev. (mm)	Dominant width (mm)[a]	#grains	Area (mm²)	Slope[b]	Intercept[b]	R²[b]	Bin range
Los Angeles 1	0.378	0.28	0.204	313	280.3	−4.90	1.66	0.970	.3–1.5
Los Angeles 2	0.378	0.27	0.211	169	49.2	−4.74	3.34	0.964	.2–1.1
Y980459 pyx	0.063	0.04	0.021	1657	23.9	−48.71	12.10	0.998	.075–.25
EETA lith A[c]	0.128	0.07	0.041	841	82.1	−24.14	8.36	0.992	.1–.45
Dhofar 019[d]	0.156	0.09	0.056	1802	190.0	−17.82	7.34	0.998	.1–.6
DaG 476[c]	0.082	0.05	0.032	716	21.6	−30.84	9.92	0.994	.1–.35
EETA lith B[c]	0.288	0.16	0.093	565	303.2	−10.72	5.12	0.996	.3–.9
QUE 94201[c]	0.390	0.24	0.222	149	139.1	−4.50	1.59	0.981	.2–.9
Y980459 ol	0.125	0.15	0.037	171	56.1	−26.98	6.06	0.998	0.1–0.25
						−15.21	4.07	0.846	0.1–0.4
Dhofar 019 ol[d]	0.173	0.09	0.051	700	289.2	−19.49	6.18	0.975	.15–.55

[a] dominant width $= G\tau = 1/$slope.

[b] Based on weighted least squares regression for designated bin range only.

[c] From Lentz and McSween (2000).

[d] From Lentz *et al.* (2001).

4.1.   Yamato 980459

Pyroxene grains in the groundmass of Y980459 produce a steeply linear plot, with only a very minor turnover at the smallest bin sizes (Fig. 5a).   The steepness of the plot reflects the overall fine grain size of the section, on average 0.06 mm and dominated by grains in the 0.02 mm size range (Table 1).   These results are very similar to those presented by Greshake *et al*. (2004), who report average and dominant sizes of 0.07 and 0.03, although their CSD plots were somewhat different from ours.   They showed a significant turnover across the three smallest bin sizes and small deviations from linearity throughout.   To verify that these differences are not just a matter of having chosen different bin sizes in calculating the CSD plots, we show in Fig. 5a how our data plots using two different bin sizes (0.015 mm and 0.025 mm).   The two plots agree strongly in shape and slope (-46.9 *vs.* -48.7), while the plot of Greshake *et al*. (2004) has a much shallower slope of -29.8.   Details of their measurement technique were not presented, so we cannot evaluate whether these differences are due to analysis technique or heterogeneities between thin sections.

The other major phase of the groundmass in Y980459 is olivine, which reportedly grew concurrently and in equilibrium with the pyroxene (Greshake *et al*., 2004; Koizumi *et al*., 2004).   We therefore conducted an analysis of olivine as well, although there are fewer olivine grains in our thin section (171) than is clearly statistically significant (*i.e.*, greater than a few hundred).   Despite some noise, our results (Fig. 5b) are similar to those presented by Greshake *et al*. (2004) (who reportedly measured only 88 olivine grains), with a steep slope at sizes smaller than 0.25 mm and a shallowing slope across the next several bins up to 0.4 mm.   There is then a large gap in grain sizes with only four grains larger than 0.85 mm, which are the megacrysts with Mg-rich cores.
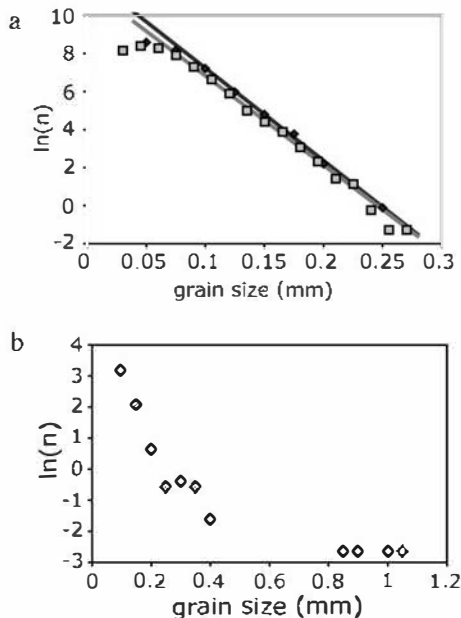

Fig. 5.   CSD plots of Yamato 980459.   a) Pyroxene size distribution using two different bin sizes: 0.025 mm (black diamonds and line) and 0.015 mm (gray squares and line) for comparison.   Line fits are weighted linear regressions.   b) Olivine CSD plot, including four megacrysts which are clearly much larger than the rest of the population.

4.2. Los Angeles

The two Los Angeles stones exhibit quite different CSD plots (Fig. 6) from that of Y980459. The grain size range is much larger, up to 1.5 mm, yielding larger average sizes of 0.38 mm and dominant sizes around 0.2 mm (Table 1). It is interesting to note that while visually Stone 2 appears slightly finer-grained than Stone 1 (Fig. 3a, b), statistically they are identical in average pyroxene grain size (Table 1). However, Stone 2 has more pyroxene grains per unit area ($3.4/mm^2$) than does Stone 1 ($1.1/mm^2$), suggesting perhaps that plagioclase is finer-grained. This higher number density is reflected in the CSD plots (Fig. 6), where Stone 2 is offset upwards (higher $ln(n)$) from Stone 1.
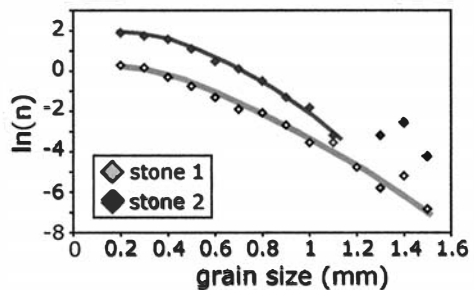

Fig. 6. Pyroxene size distributions for the two stones of Los Angeles. Curves are hand drawn approximations of plot shapes. Note that the plots have a similar curvature for most grain sizes.

Unlike Y980459 but similar to QUE 94201 (Lentz and McSween, 2000), the Los Angeles CSD plots have a subtle but clear concave-down curvature. Weighted linear fits were calculated for the two plots, by the same technique mentioned above, but the R^2 values (0.970 and 0.964) of the line fits show that indeed these plots are not as linear as those of Y980459 ($R^2 = 0.998$) and other picritic shergottites (Table 1). When curves are drawn to the data, it is apparent that over most of the grain size range, the two plots are parallel, with Stone 2 becoming slightly steeper before the plot becomes more noisy at the largest grain sizes (represented by only three grains wider than 1.1 mm).

5. Discussion and comparisons to other shergottites

This study is part of an ongoing attempt to quantify the crystallization histories of the basaltic shergottites, so the results need to be placed into context with previously described shergottites.

5.1. Yamato 980459

Mineralogically, Y980459 is most like the other picritic shergottites, and this holds true for its textural character as well. Figure 7a compares CSD plots of groundmass pyroxenes in Y980459, DaG 476, EETA79001A, and Dhofar 019. Despite the fact that the Yamato pyroxenes are mostly orthopyroxene, there is a decided similarity. All four plots are linear, as demonstrated by high R^2 values associated with line fits (Table 1;
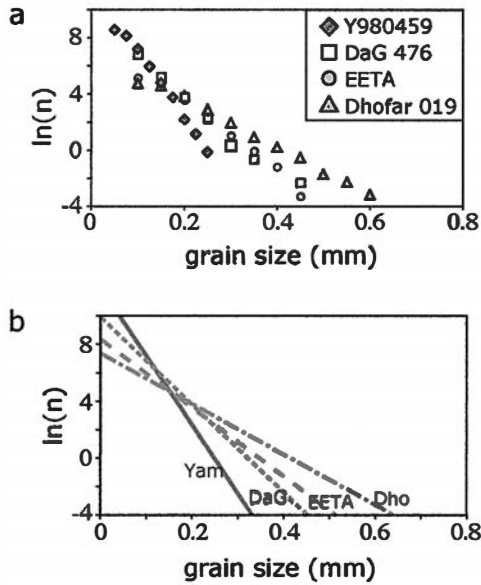
Fig. 7. Picritic shergottite CSD plots. a) CSDs of pyroxene groundmass grains in Y980459 compared to other picritic shergottites. Note how linear all plots are, with only minor turnovers at the smallest sizes. b) Weighted linear fits to CSD plots shown in a. Note how much steeper Y980459 is than the other shergottites, reflecting its faster cooling rate.

Fig. 7b), implying that the pyroxene populations in all the groundmasses were grown in one stage under steady-state conditions of nucleation and growth.   All four show a limited size range, reaching at most 0.6 mm across (in Dhofar 019), implying a limited growth period.   Y980459 presents the steepest plot, consistent with previous interpretations, and the lack of maskelynite and phosphates, that it cooled rapidly beyond its initial olivine growth stages.

An important relationship in CSD theory is that the slope of the line (m) is related to growth rate (G) and residence time (τ) of the population by:

$$m = -1/G\tau.$$

This means that if we know either how long the grains grew or how quickly they grew, we can use the CSD slope to estimate the other value.

Lentz and McSween (2000) showed that using olivine zoning (Mikouchi *et al.*, 1999) and experimentally derived growth rates (McCoy and Lofgren, 1999) to constrain the histories of DaG 476 and EETA79001A, the groundmass pyroxenes of these two picritic shergottites cooled at a rate of ~2–3°C/hr and grew at about 8.4e⁻8 mm/s. The fact that the CSD slope for Y980459 is steeper than those for either DaG 476 or EETA79001A (Table 1; Fig. 7b) suggests that either the growth rate is much slower or the growth time even shorter.   Since the groundmass bulk composition is fairly similar, it seems likely that the growth rate of the pyroxenes would be similar, too.

Using the above G, then, the CSD slope gives a growth time (τ) of 2.8 days (compared to 4.5 days for DaG 476 and 5.7 days for EETA79001A; Lentz and McSween, 2000).   For the temperature range over which the pyroxene was growing, this would imply a cooling rate of 3°C/hr (1360°–1150°) to 7°C/hr (1360°–900°), depending on whether the final quenching event occurred before the plagioclase liquidus

was reached (~1150°C; Koizumi *et al*., 2004) or substantially after. McKay *et al*. (2004) report that they experimentally produced textures similar to those in Y980459 (*e.g*. large olivine grains, elongate pyroxene grains, and interstitial glass with some skeletal mafic crystals) with a constant cooling rate of 5°C/hr from 1460°–900°C, consistent with our calculated rates. However, regardless of whether plagioclase was suppressed due to rapid quenching or substantial undercooling, Greshake *et al*. (2004) argue that a final quenching event is necessary to account for textures of the dendritic and swallow-tail olivines in the glassy mesostasis, with cooling on the order of 1450°C/hr or faster.

In fact, a common process in basaltic fields may account for these two last stages of fast and then very rapid cooling. Often during inflation of a basaltic field, discreet uplifted mounds, called tumuli (Walker, 1991; Hon *et al*., 1994), are formed within the flow field. The lava within these tumuli may sit for some time (days to months) before pressure builds up sufficiently for the lava to break through the crust and erupt through the tumulus. Such a scenario could explain the fast cooling of the groundmass associated with shallow burial (*i.e.* < few m), followed by a sudden rapid quenching of the remaining melt into a glassy matrix.

We also analyzed the olivine population using CSD and as stated above, the rough shape of the plot is steep at the smallest sizes and gradually shallows with increasing size. A line fit to the steepest linear segment produces a moderate slope of −26.98. This segment corresponds to the latest of the olivine grains to grow (*i.e.* the smallest) and covers a similar range of sizes as the groundmass pyroxene grains (up to 0.25 mm). Compositionally, the orthopyroxene and olivine grains of the groundmass grew in equilibrium (Greshake *et al*., 2004), implying concurrent growth under the same conditions. The fact that the slopes of the pyroxene and olivine CSDs do not agree, points to different growth rates for the two phases: olivine grew about 1.8 times faster than pyroxene, or at 1.5e–7 mm/s, based on our growth rate estimate above. Alternatively, if all the olivine grains up to the 0.4 mm size bin grew concurrently with the pyroxene and over the same time interval, then a faster average growth rate would be necessary to account for the even shallower slope: ~2.7e–7 mm/s.

For comparison, Fig. 8 shows a CSD plot of the Dhofar 019 olivine population superimposed on the Y980459 plot (data from Lentz *et al*., 2001; Taylor *et al*., 2002). While the Dhofar plot shows a similar relationship of two apparently separate populations (the smaller up to 0.5 mm and then several outsized megacrysts), there is no apparent shallowing of the Dhofar plot through the smaller population size range.
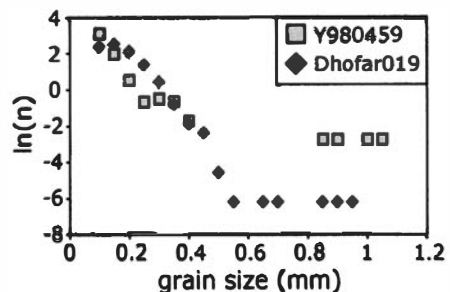

Fig. 8. *CSDs of olivine grains in Yamato 980459 and Dhofar 019, including a few (4 and 3 respectively) outsized megacrysts much larger than the rest of the populations. Note that the plot for Y980459 represents far fewer grains (171) than for Dhofar 019 (700).*

There is also a small turnover at the smallest size bin in the Dhofar plot, implying some minor post-nucleation growth of the population, or absorption of the smallest grains during subsolidus ripening.   Also in contrast to Y980459, there is much closer agreement between the slopes of the olivine and pyroxene plots from Dhofar 019 (respectively, -19.5 and -17.8), suggesting more similar growth rates for the two silicates under those less compositionally primitive conditions.

5.2. Los Angeles

Both Los Angeles stones exhibit simple CSD plots which, while curved, imply one continuous period of growth for the pyroxene populations.   They are remarkably similar to the curved plots of other shergottites with evidence of co-crystallization of plagioclase and pyroxene, QUE 94201 and EETA79001B (Figs. 6, 9).   Our previous interpretation for the shapes of the QUE 94201 and EETA79001B plots was that the downward curvature represented a paucity of larger grains due to interference between the co-crystallizing phases (Lentz and McSween, 2000).   The fact that the two stones of Los Angeles also exhibit the subophitic, intergrown texture of co-crystallizing phases and curved CSD plots lends credence to this interpretation.   Variations in the curvature of these plots likely reflects the magnitude of the plagioclase effect, resulting from variable plagioclase to pyroxene proportions.   EETA79001B has the lowest plagioclase: pyroxene ratio of the four samples (0.52) and displays the steepest of the curves (Fig. 9), which becomes nearly linear at the largest sizes.   In comparison, the plots for QUE 94201 and the two Los Angeles stones are very similar in curvature and steepness, and all three show similar plagioclase: pyroxene ratios (1.05, 1.16, and1.02, respectively).

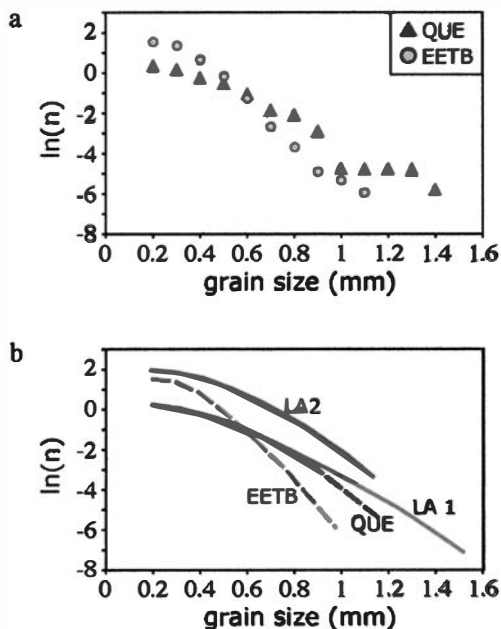Warren *et al*. (2004) speculate that the increased abundance of PBM in Los

Fig. 9. *Co-saturated shergottite CSDs. a) Previously measured CSDs of EETA79001 lithology B and QUE 94201, presented for comparison with Los Angeles CSDs (Fig. 6). b) Hand drawn curves illustrating the similarities and differences between the four co-saturated shergottite stones. Note the overlap of QUE and LA Stone 1 for most grain sizes, but that QUE and LA Stone 2 are nearly parallel throughout.   EETA79001B is substantially steeper than the rest.*

Angeles Stone 2 is due to slight compaction either pushing extra crystals into the Stone 1 vicinity or pushing late-stage melt into the Stone 2 vicinity. The fact that the CSD plot for Stone 1 is such a smooth curve with no upturn at larger sizes suggests there was no late adjustments to the population distribution. This makes more likely the idea that late-stage melt migration is responsible for the additional PBM in Stone 2. Formation of segregation veins from late-stage melt migration is common in basalt flows only a few meters thick (*e.g.*, Dungan *et al*., 1986; Self *et al*., 1996), so no substantial compression is necessary to produce the minor modal differences measured between the two Los Angeles stones.

Unfortunately, the curvature of the Los Angeles CSD plots makes it unfeasible to obtain an estimate of growth time or cooling rate, since the line fits are just a rough estimate. But the simplicity of the plots (with no extra humps or jags) supports the idea that these pyroxene populations underwent a single continuous growth period with steady-state conditions, perhaps in a thick surface flow or a shallow intrusion. While the CSD information does not let us directly learn anything about the growth of the pyroxferroite, we can substantiate that it is a late-stage modification which does not influence the primary growth period of the pyroxene.

6.   Conclusions

Los Angeles and Yamato 980459 represent the compositional end members of the known basaltic shergottites, the most evolved and the most primitive respectively, but their crystallization histories are very similar to other basaltic shergottites.

Y980459 must have begun cooling slowly at depth, while the olivine megacrysts grew, but then, according to the olivine CSD, a shift in crystallization conditions occurred, probably associated with the magma rising to the surface. Groundmass olivine and pyroxene then began to nucleate and crystallize, together. Unlike the model of Greshake *et al*. (2004), we suggest that the groundmass olivine and pyroxene did not growth at depth, but experienced faster cooling rates upon ascent and emplacement (3–7°C/hr) on the surface, perhaps within a several-meter high tumulus. The final quenching event, which produced the glassy mesostasis and associated dendritic phases, could be explained by a subsequent eruption of the semi-crystalline lava from within the tumulus into the open air.

The pattern of olivine megacryst growth in magma chamber conditions, followed by ascent and eruption, with a pyroxene-rich groundmass grown at shallow depths or within thick flows is common to all the picritic shergottites. The main variables between the meteorite samples seem to be the rapidity of groundmass growth (which likely reflects the original depth of the sample within the final flow) and the source of the megacrysts (either primary phenocrysts or scrounged xenocrysts from previous magmatic batches).

Los Angeles compares well with a different textural type, one that resembles terrestrial basalts much more closely with its subophitic intergrowth of co-crystallized pyroxene and plagioclase. Despite the prevalence of the PBM, the CSD of pyroxene, which still dominates modally, shows a very similar crystallization history to that of QUE 94201: a single continuous stage of crystallization, probably in a shallow intrusion

or deep within a moderately thick lava flow. And like Y980459, Los Angeles also demonstrates a typical basaltic process of minor late-stage melt migration, slightly enriching restricted portions of a common flow.

Acknowledgments

References

Barrat, J.A., Jambon, A., Bohn, M., Gillet, Ph., Sautter, V., Göpel, C., Lesourd, M. and Keller, F. (2002): Petrology and chemistry of the picritic shergottite North West Africa 1068 (NWA 1068). Geochim. Cosmochim. Acta, **66**, 3505–3518.

Cashman, K.V. and Marsh, B.D. (1988): Crystal size distribution (CSD) in rocks and the kinetics and dynamics of crystallization: II. Makaopuhi lava lake. Contrib. Mineral. Petrol., **99**, 292–305.

Dungan, M.A., Lindstrom, M.M., McMillan, N.J., Moorbath, S., Hoefs, J. and Haskin, L.A. (1986): Open system magmatic evolution of the Taos Plateau volcanic field, northern New Mexico: 1. The petrology and geochemistry of the Servilleta basalt. J. Geophys. Res., **91** (B6), 5999–6028.

Friedman, R.C. (1998): Petrologic clues to lava flow emplacement and post-emplacement processes. PhD dissertation, University of Hawaii, Honolulu, USA. 260 p.

Friedman-Lentz, R.C., Tayor, G.J. and Treiman, A.H. (1999): Formation of a martianpyroxenite: a comparative study of the nakhlite meteorites and Theo's Flow. Meteorit. Planet. Sci., **34**, 919–932.

Goodrich, C.A. (2002): Petrogenesis of olivine-phyric shergottites Sayh al Uhaymir 005 and Elephant Moraine A79001 lithology A. LPI Contribution No. 1134, Un-mixing SNCs, 17–18.

Greshake, A, Fritz, J. and Stoffler, D. (2004): Petrology and shock metamorphism of the olivine-phyric shergottite Yamato 980459: Evidence for a two-stage cooling and a single-stage ejection history. Geochim. Cosmochim. Acta, **68**, 2359–2377.

Grossman, J.N. and Zipfel, J. (2001): The Meteoritical Bulletin, No. 85, 2001 September. Meteorit. Planet. Sci., **36**, A293–A322.

Hale, V.P.S., McSween, H.Y., Jr. and McKay, G.A. (1999): Re-evaluation of intercumulus liquid composition and oxidation state for the Shergotty meteorite. Geochim. Cosmochim. Acta, **63**, 1459–1470.

Helz, R.T., Kirschenbaum, H. and Marinenko, J.W. (1989): Diapiric transfer of melt in Kilauea Iki lava lake, Hawaii: A quick, efficient process of igneous differentiation. GSA Bull., **101**, 578–594.

Hon, K., Kauahikaua, J., Denlinger, R. and Mackay, K. (1994): Emplacement and inflation of pahoehoe sheet flows: Observations and measurements of active lava flows on Kilauea Volcano, Hawaii. GSA Bull., **106**, 351–370.

Ikeda, Y., Takeda, H., Kimura, M and Nakamura, N. (2002): A new basaltic shergottite, Dhofar 378. Antarctic Meteorites XXVII. Tokyo, Natl Inst. Polar Res., 40–42.

Irving, A.J., Kuehner, S.M., Hupé, A.C. and Hupé, G.M. (2002): Olivine-phyric basaltic shergottite NWA 1195: a very primitive Martian lava. Meteorit. Planet. Sci., **37** (Suppl.), A69.

Jambon, A., Barrat, J.A., Sautter, V., Gillet, Ph., Göpel, C., Javoy, M., Joron, J-L. and Lesourd, M. (2002): The basaltic shergottite North West Africa 856: Petrology and chemistry. Meteorit. Planet. Sci., **37**, 1147–1164.

Jambon, A., Bohm, M., Boudouma, O., Chennaoui-Aoudjehane, H. and Franchi, I. (2003): Al Mala'ika (NWA 1669): A new shergottite from Morocco/mineralogy and petrology. Meteorit. Planet. Sci., **38**

(Suppl.), A43.

Koizumi, E., Mikouchi, T., Miyamoto, M., McKay, G., Monkawa, A. and Chokai, J. (2004): Experimental and computational studies of the olivine-phyric shergottite Yamato 980459. Antarctic Meteorites XXVIII. Tokyo, Natl Inst. Polar Res., 39–40.

Lentz, R.C.F. and McSween, H.Y., Jr. (2000): Crystallization of the basaltic shergottites: Insights from crystal size distribution (CSD) analysis of pyroxenes. Meteorit. Planet. Sci., **35**, 919–927.

Lentz, R.C.F., McSween, H.Y., Jr., Nazarov, M.A. and Taylor, L.A. (2001): A textural consideration of Dhofar 019 with comparisons to other basaltic shergottites. Lunar and Planetary Science XXXII. Houston, Lunar Planet. Inst., Abstract #1742, (CD-ROM).

Mangan, M.T., Cashman, K.V. and Newman, S. (1993): Vesiculation of basaltic magma during eruption. Geology, **21**, 157–160.

Marsh, B.D. (1988): Crystal size distribution (CSD) in rocks and the kinetics and dynamics of crystallization: I. Theory. Contrib. Mineral. Petrol., **99**, 277–291.

Marsh, B.D. (1998): On the interpretation of crystal size distributions in magmatic systems. J. Petrol., **39**, 553–599.

McCoy, T.J. and Lofgren, G. (1999): Crystallization of the Zagami shergottite: and experimental study. Earth Planet. Sci. Lett., **173**, 397–411.

McCoy, T.J., Taylor, G.J. and Keil, K. (1992): Zagami: Product of a two-stage magmatic history. Geochim. Cosmochim. Acta, **56**, 3571–3582.

McKay, G., Le, L., Schwandt, C., Mikouchi, T. and Koizumi, E. (2004): Redox state and petrogenesis of Martian basalts: Clues from experimental petrology. Antarctic Meteorites XXVIII. Tokyo, Natl Inst. Polar Res., 44–45.

McSween, H.Y., Jr., Eisenhour, D.D., Taylor, L.A., Wadhwa, M. and Crozaz, G. (1996): QUE 94201 shergottite: Crystallization of a martian basaltic magma. Geochim. Cosmochim. Acta, **60**, 4563–4569.

Meyer, C. (2003): Mars meteorite compendium. http://www-curator.jsc.nasa.gov/curator/antmet/mmc/mmc.htm, NASA Johnson Space Center.

Mikouchi, T., Miyamoto, M. and McKay, G.A. (1999): Cooling rates of olivine in the Martian meteorites Dar al Gani 476 and Elephant Moraine 79001. Meteorit. Planet. Sci., **34** (Suppl.), A81–A82.

Mikouchi, T., Koizumi, E., McKay, G., Monkawa, A., Ueda, Y. and Miyamoto, M. (2003): Mineralogy and petrology of the Yamato 980459 Martian meteorite: A new shergottite-related rock. International Symposium—Evolution of Solar System Materials: A New Perspective from Antarctic Meteorites. Tokyo, Natl Inst. Polar Res., 82–83.

Misawa, K. (2003): The Yamato 980459 shergottite consortium. International Symposium—Evolution of Solar System Materials: A New Perspective from Antarctic Meteorites. Tokyo, Natl Inst. Polar Res., 84–85.

Philpotts, A.R., Carroll, M. and Hill, J.M. (1996): Crystal-mush compaction and the origin of pegmatitic segregation sheets in a thick flood-basalt flow in the Mesozoic Hartford Basin, Connecticut. J. Petrol., **37**, 811–836.

Rubin, A.E., Warren, P.H., Greenwood, J.P, Verish, R.S., Leshin, L.A., Hervig, R.L., Clayton, R.N. and Mayeda, T.K. (2000): Los Angeles: The most differentiated basaltic Martian meteorite. Geology, **28**, 1011–1014.

Self, S., Thordarson, Th., Keszthelyi, L., Walker, G.P.L., Hon, K., Murphy, M.T., Long, P. and Finnemore, S. (1996): A new model for the emplacement of Columbia River basalts as large, inflated pahoehoe lava flow fields. Geophys. Res. Lett., **23**, 2689–2692.

Steele, I.M. and Smith, J.V. (1982): Petrography and mineralogy of two basalts and olivine-pyroxene-spinel fragments in achondrite EETA79001. Proc. Lunar Planet. Sci. Conf., 13th, Pt. 1, A375–A384 (J. Geophys. Res. **87** Suppl).

Stolper, E.M. and McSween, H.Y., Jr. (1979): Petrology and origin of the shergottite meteorites. Geochim. Cosmochim. Acta, **43**, 1475–1498.

Taylor, L.A., Nazarov, M.A., Ivanova, M.A., Patchen, A., Clayton, R.N. and Mayeda, T.K. (2000): Petrology of the Dhofar 019 shergottite. Meteorit. Planet. Sci., **35** (Suppl.), A155.

Taylor, L.A., Nazarov, M.A., Shearer, C.K., McSween, H.Y. Jr. *et al.* (2002): Martian meteorite Dhofar 019:

a new shergottite. Meteorit. Planet. Sci., **37**, 1107–1128.

Wadhwa, M., McSween, H.Y., Jr. and Crozaz, G. (1994): Petrogenesis of shergottite meteorites inferred from minor and trace element microdistributions. Geochim. Cosmochim. Acta, **58**, 4213–4229.

Walker, G.P.L. (1991): Structure and origin by injection of lava under surface crust, of tumuli, "lava rises", "lava-rise pits", and "lava-inflation clefts" in Hawaii. Bull. Volcanol., **53**, 546–558.

Warren, P.H., Greenwood, J.P. and Rubin, A.E. (2004): Los Angeles: A tale of two stones. Meteorit. Planet. Sci., **39**, 137–156.

Zipfel, J. (2000): Sayh al Uhaymir 005/008 and its relationship to Dar al Gani 476/489. Meteorit. Planet. Sci., **35** (Suppl.), A178.

Zipfel, J., Scherer, P., Spettel, B., Dreibus, G. and Schultz, L. (2000): Petrology and chemistry of the new shergottite Dar al Gani 476. Meteorit. Planet. Sci., **35**, 95–106.